nature geoscience

ARTICLES

PUBLISHED ONLINE: 1 AUGUST 2016 | DOI: 10.1038/NGEO2774

Earthquake nucleation in weak subducted carbonates

Robert M. Kurzawski[1,2*], Michael Stipp[1], André R. Niemeijer[3], Christopher J. Spiers[3] and Jan H. Behrmann[1]

Ocean-floor carbonate- and clay-rich sediments form major inputs to subduction zones, especially at low-latitude convergent plate margins. Therefore, knowledge of their frictional behaviour is fundamental for understanding plate-boundary earthquakes. Here we report results of mechanical tests performed on simulated fault gouges prepared from ocean-floor carbonates and clays, cored during IODP drilling offshore Costa Rica. Clay-rich gouges show internal friction coefficients (that is, the slope of linearized shear stress versus normal stress data) of $\mu_{int} = 0.44 - 0.56$, irrespective of temperature and pore-fluid pressure (P_f). By contrast, μ_{int} for the carbonate gouge strongly depends on temperature and pore-fluid pressure, with μ_{int} decreasing dramatically from 0.84 at room temperature and $P_f = 20$ MPa to 0.27 at $T = 140$ °C and $P_f = 120$ MPa. This effect provides a fundamental mechanism of shear localization and earthquake generation in subduction zones, and makes carbonates likely nucleation sites for plate-boundary earthquakes. Our results imply that rupture nucleation is prompted by a combination of temperature-controlled frictional instability and temperature- and pore-pressure-dependent weakening of calcareous fault gouges.

Calcareous sediments form an important part of the global sediment budget, especially at low latitudes where carbonates make up to >90% of marine sediments[1]. These sediments are deposited on continental shelves and slopes, and on young and buoyant oceanic plates. Thus, calcareous sediments may end up within a subduction channel at convergent plate boundaries, either by direct subduction with the downgoing oceanic plate, or by tectonic erosion of a forearc system. This means that the mechanical properties of calcareous sediments can potentially influence the development of the plate-boundary décollement and the transition between brittle (potentially seismic) and ductile (aseismic) deformation. The classical view is that nucleation of large plate-boundary earthquakes is limited to the so-called seismogenic zone, located at depths between ~10 and 40 km at most active continental margins[2–4]. Parameters and processes controlling especially the updip limit of the seismogenic zone are not satisfactorily characterized to date, and remain a matter of debate. Phenomena occurring in this environment, such as incidence of shallow seismogenesis, tsunamigenic earthquakes and slow slip events, have been attributed to the presence or absence of overpressured fluids[5–8], and to the frictional properties of subduction channel materials[9–15]. Here, we report experiments on subduction zone input materials cored during IODP (Integrated Ocean Drilling Program) Expedition 344 offshore Costa Rica, with the specific goal of assessing the frictional response to pore-fluid-pressure variations within the range of normal stress and temperature conditions relevant for shallow seismogenesis.

The Costa Rica Seismogenesis Project (CRISP) encompassing IODP Expeditions 334 and 344 investigates the genesis of large earthquakes and related tsunamis at a tectonically erosive active continental margin. Subduction erosion, that is, the basal tectonic removal of overriding plate material, occurs along the entire Middle America Trench[16–18] (MAT), where the oceanic Cocos Plate is subducted beneath the Caribbean Plate. The MAT is the site of extensive subduction of calcareous sediments. Nannofossil calcareous ooze deposits, up to hundreds of metres thick, are intercalated with or covered by hemipelagic clayey sediments and have been reported along the trench between Guatemala (Deep-Sea Drilling Program Legs 67 and 69)[19] and as far south as the Nazca Plate[20]. In this study, sample material from CRISP was sheared experimentally to characterize the frictional behaviour of clayey and carbonate-rich sediments at sliding velocities low enough to study rupture nucleation.

Sample material and experiment design

Simulated fault gouges were prepared from two prominent lithological units within the sedimentary cover sequence of CRISP Site U1414 (Expedition 344) on the Cocos Plate[21]: calcareous nannofossil-rich clay (Unit IB); and alternating nannofossil-rich calcareous ooze and sponge-spicule-rich calcareous ooze (Unit IIB)[21]. Between the two units there is a marked difference in carbonate content. Hemipelagic material from Core U1414-14H (Unit IB) shows carbonate contents <20 wt% and further contains quartz, feldspar, clay minerals and opal-A (Supplementary Fig. 1; D. Charpentier, personal communication, 2015). By contrast, calcareous ooze from Core U1414-30X (Unit IIB) contains >85 wt% carbonate, and minor diagenetically altered opal-CT plus accessory halite. Opal contents of ~5 wt% remain constant over most parts of the stratigraphic succession (D. Charpentier, personal communication, 2015).

Friction experiments were conducted in a hydrothermal rotary shear apparatus[22] at room temperature, 70 °C and 140 °C, using fixed pore-fluid pressures of 20, 60 and 120 MPa, to target consecutive thermal domains across the updip limit of the seismogenic zone (Table 1). Depending on the local thermal gradient, these domains are spatially shifted implying variations in the amount of

[1]Department of Marine Geodynamics, GEOMAR Helmholtz Centre for Ocean Research Kiel, Wischhofstr. 1-3, 24148 Kiel, Germany. [2]Institute of Geosciences, University of Kiel, Ludewig-Meyn-Str. 10, 24118 Kiel, Germany. [3]HPT Laboratory, Department of Earth Sciences, Utrecht University, Budapestlaan 4, 3484 CD, Utrecht, The Netherlands. *e-mail: rkurzawski@geomar.de

Table 1 | List of experiments and experimental conditions applied during each experiment.

Experiment	σ_n^{eff} (MPa)	T (°C)	P_f (MPa)	μ_{int}
Hemipelagic silty clay gouge				
1414-14H6-RT20	30-50-70-90-110	Room temperature	20	0.56 (Fig. 2a)
1414-14H6-RT120	30-50-90-110	Room temperature	120	0.44 (Fig. 2c)
1414-14H6-7060	30-50-70-90-110	70	60	0.55 (Fig. 2b)
1414-14H6-14060	30-50-90-110	140	60	0.46 (Fig. 2b)
1414-14H6-140120	30-50-70-90-110	140	120	0.46 (Fig. 2c)
Calcareous ooze gouge				
1414-30X7-RT20	30-50-70-90-110	Room temperature	20	0.84 (Fig. 2d)
1414-30X7-RT60	30-50-70-110	Room temperature	60	0.58 (Fig. 2e)
1414-30X7-RT120	30-50-90-110	Room temperature	120	0.58 (Fig. 2f)
1414-30X7-7060	30-50-70-90-110	70	60	0.58 (Fig. 2e)
1414-30X7-14020	30-50-90-110	140	20	0.52 (Fig. 2d)
1414-30X7-14060	30-50-90-110	140	60	0.54 (Fig. 2e)
1414-30X7-140120	30-50-70-90-110	140	120	0.27 (Fig. 2f)
1414-30X7-140120*i*	30-50-70-90-110	140	120	0.42 (Fig. 2f)

overburden and hence the (effective) normal stress σ_n^{eff}. Frictional behaviour was explored by stepwise increase of effective normal stress from 30 MPa to 110 MPa, and by applying slip velocity steps of 10-1-3-10-30-100 µm s^{-1} (Fig. 1a), to obtain the velocity dependence of sliding friction. The apparent coefficient of sliding friction is expressed as the ratio of shear stress over effective normal stress assuming no cohesion (τ/σ_n^{eff}). Frictional response to instantaneous changes in shearing velocity is interpreted on the basis of rate- and state-dependent friction (RSF) theory[23,24], whereby the key parameter (a–b):

$$(a-b) = \Delta(\tau/\sigma_n^{eff})/\Delta \ln V \quad (1)$$

describes the velocity (V) dependence of friction. This indicates whether the tested material shows velocity-weakening ($a-b<0$) or velocity-strengthening ($a-b>0$) behaviour at each specific set of experimental conditions (Fig. 1a,b). Velocity-strengthening behaviour results in stable, continuous slip, whereas velocity weakening results in slip instability, if elastic stiffness (K) of the loading system is below its critical value (K_{crit}) specified as

$$K < K_{crit} = \sigma_n^{eff}(b-a)/D_c \quad (2)$$

where D_c is the critical slip distance[25]. Laboratory stick–slip frictional instability has long been considered an analogue for natural earthquakes[26]. During the sticking phase a continuous shear stress build-up occurs on locked shearing surfaces until the stored energy radiates in a quasi-instantaneous slip event accompanied by a stress drop, and the cycle recommences (Fig. 1c). Stress drop and recurrence time are important characteristics to study such behaviour in detail. Here, we seek the conditions at which slip instabilities are triggered and hence nucleation of earthquakes is favoured.

Besides the apparent friction coefficient (τ/σ_n^{eff}), the internal friction coefficient μ_{int} was determined for each experiment using a linear regression of steady-state shear stress at a velocity of 10 µm s^{-1} against effective normal stress (Supplementary Fig. 4), that is, by best-fitting the Mohr–Coulomb criterion:

$$\tau = \mu_{int}\sigma_n^{eff} + c \quad (3)$$

where c is the cohesion. By definition, RSF laws apply to dynamic slip on a fault plane. The internal friction coefficient, however, characterizes the normal stress-dependent shear strength at the point of static rock failure or reshearing of healed fault rock, that is, strength at the transition from elastic to (Coulomb) plastic strain. Plastic strain initiation in frictionally unstable material is integral to earthquake nucleation. Therefore, quasi-static frictional strength (μ_{int}) and the slip dependence and especially the velocity dependence of dynamic friction (τ/σ_n^{eff}) are the key factors that

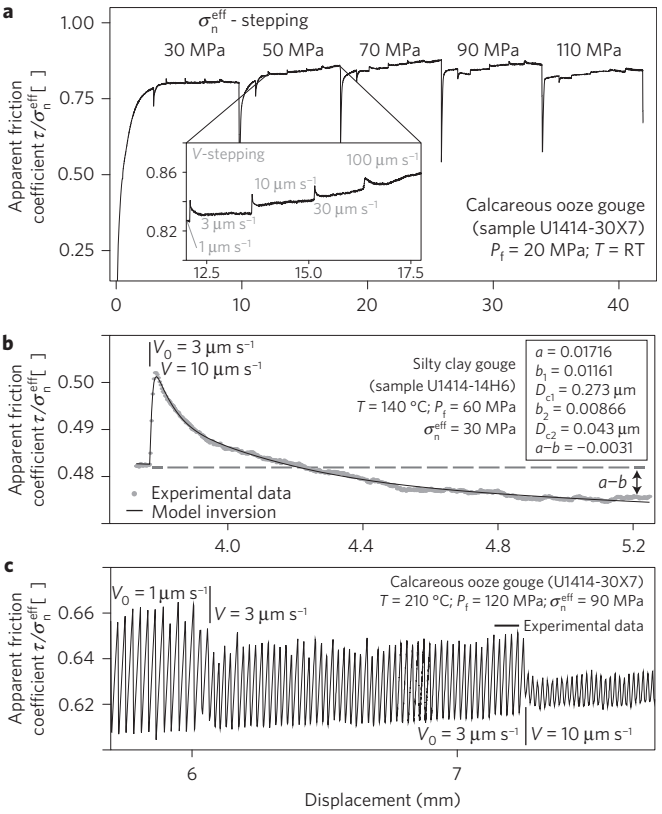

Figure 1 | Representative records of velocity-stepping experiments. **a**, Calcareous ooze gouge deformed at room temperature (RT) and 20 MPa pore-fluid pressure (P_f); effective normal stress (σ_n^{eff}) and velocity (V) steps are labelled. **b**, Experimental data and model fit for a single velocity step of silty clay gouge at 10 µm s^{-1}, 140 °C and an effective normal stress of 30 MPa. RSF parameters from inversion results are given in the inset; the material is velocity weakening as indicated by negative (a–b). **c**, Unstable slip, that is, 'stick–slip' events, of calcareous ooze gouge at 210 °C and effective normal stress of 90 MPa.

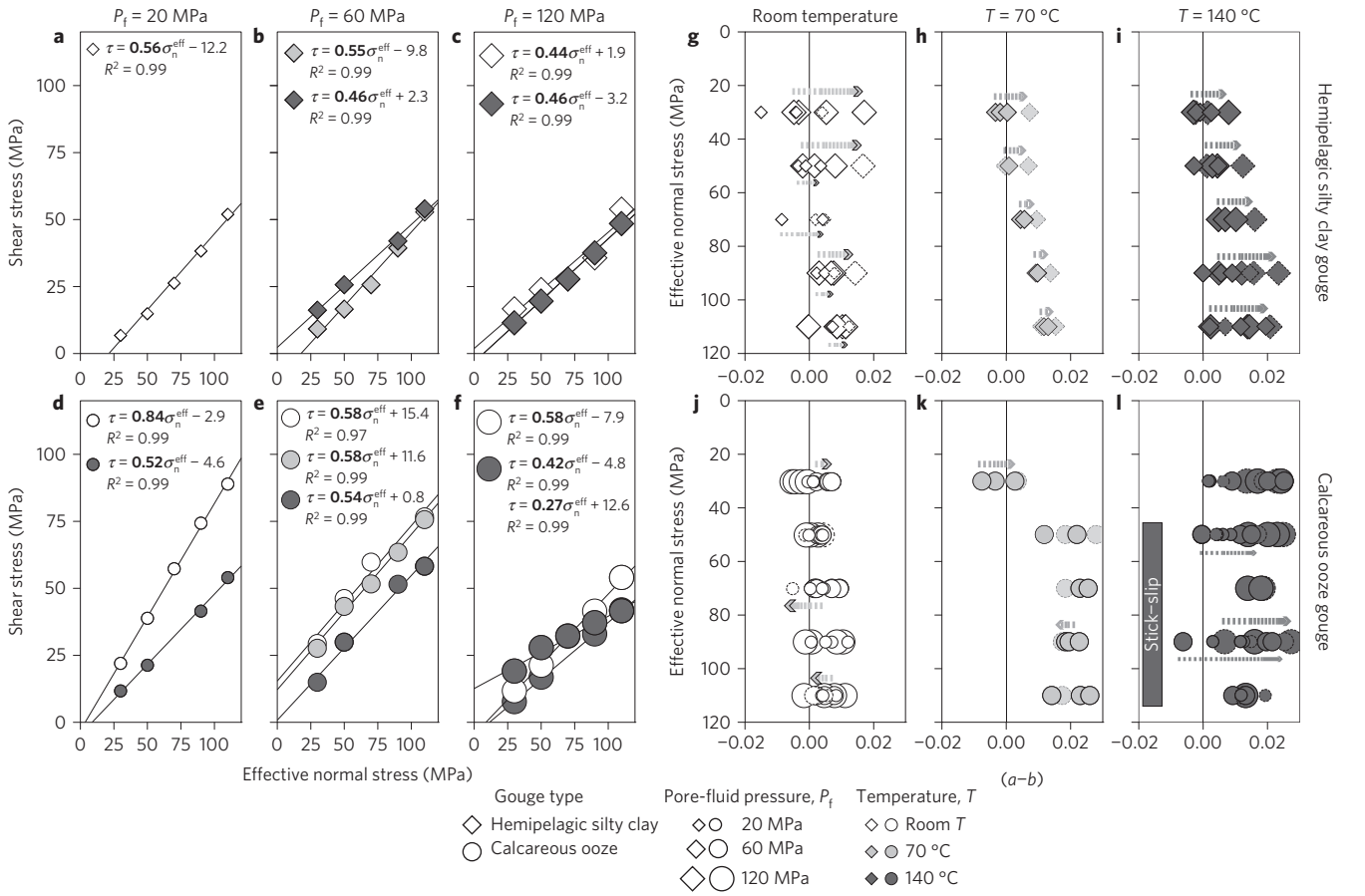

Figure 2 | Mechanical data of hemipelagic silty clay (upper panels) and calcareous ooze (lower panels), deformed under varying experimental conditions. Symbol greyscale represents temperature; symbol size represents pore pressure; and symbol shape the gouge type as indicated in the legend below panels **a**–**l**. **a**–**f**, Linear regressions of shear stress versus effective normal stress yielding internal friction values. Note the weakening of calcareous ooze as a function of temperature and pore-fluid pressure in **d**–**f**. **g**–**l**, Effective normal stress versus RSF parameter (a–b). Arrows point towards higher load point velocities if there is a systematic trend of (a–b) with V. Arrow thickness correlates with symbol size.

control the nucleation process. Henceforth, the term 'weakening', refers to weakening associated with changes in internal friction (μ_{int}), whereas weakening related to instantaneous displacement rate changes is always termed 'velocity weakening'.

Contrasting frictional behaviour in clay versus carbonate

Simulated gouge prepared from hemipelagic silty clay is weak and, in terms of internal friction, shows no significant sensitivity to temperature or pore-fluid-pressure variations. It consistently yields internal friction coefficients of $\mu_{int} \approx 0.5$ ($0.44 < \mu_{int} < 0.56$) over the entire range of conditions we explored (Fig. 2a–c). Towards lower effective normal stress and sliding velocity, (a–b) decreases from 0.023 to −0.015 at constant pore-fluid pressure (Fig. 2g–i). Moreover, (a–b) depends on sliding velocity as indicated by arrows pointing towards increasing load point velocity in Fig. 2g–i. Velocity steps showing velocity-weakening behaviour occur across the whole range of temperatures and pore-fluid pressures tested, but especially at room temperature and low pore-fluid pressure. An increase in pore-fluid pressure at constant temperature consistently results in slightly increasing (a–b) values.

Samples prepared from nannofossil-rich calcareous ooze are frictionally strong at room temperature and $P_f = 20$ MPa pore-fluid pressure, with $\mu_{int} = 0.84$ (Fig. 2d). Unlike the hemipelagic clay samples, they show a dramatic weakening effect with increases in temperature and pore-fluid pressure. Tests at $P_f = 60$ MPa and all temperatures explored show a decrease in internal friction to $\mu_{int} \approx 0.55$ ($0.54 < \mu_{int} < 0.58$). At the highest temperature and pore-fluid pressure ($T = 140$ °C; $P_f = 120$ MPa), samples derived from calcareous ooze are weaker than the hemipelagic clay, with an internal friction coefficient of $\mu_{int} = 0.27$ (Fig. 2d–f). A second experiment conducted at the same conditions but with much shorter equilibration time before shear initiation resulted in the lowest values in apparent friction coefficient ($(\tau/\sigma_n^{eff}) = 0.25$–$0.45$, compared with $(\tau/\sigma_n^{eff}) = 0.38$–$0.72$ after a longer equilibration time) and an internal friction coefficient of $\mu_{int} = 0.42$, the second lowest value (Fig. 2f and Supplementary Fig. 6). This experiment further confirms the significance of temperature- and pore-pressure-dependent weakening and in addition demonstrates that healing processes significantly affect cohesion and therefore the apparent friction coefficient (τ/σ_n^{eff}) of carbonate gouges. The internal friction coefficient (μ_{int}) shows much more consistent values. Increasing the temperature to 140 °C at low pore-fluid pressure, and increasing the pore-fluid pressure to 120 MPa at room temperature, results in a decrease in μ_{int} to 0.52–0.58 (Fig. 2d,f). This indicates intensification of overall weakening by increasing both temperature and pore pressure.

Except for the occurrence of unstable slip at 140 °C, the frictional stability of calcareous ooze samples does not show a clear dependence on temperature or pore-fluid pressure. Behaviour is velocity-neutral at room temperature and low pore-fluid pressure (20 MPa), with values between $-0.0014 \leq (a-b) \leq 0.012$. Towards higher effective normal stress and lower shearing velocities it tends to velocity-strengthen (Fig. 2j). At room temperature and 120 MPa pore pressure, calcareous ooze gouge is velocity weakening with

$-0.005 \leq (a-b) \leq -0.001$ at low effective normal stress (30 MPa, Fig. 2j). At 70 °C, the material exhibits the most marked velocity-strengthening behaviour with $0.012 < (a-b) < 0.031$, except for the lowest effective normal stress step of 30 MPa, for which velocity weakening is recorded ($-0.007 \leq (a-b) \leq 0.003$). There is no clear trend in $(a-b)$ as a function of effective normal stress or sliding velocity (Fig. 2k). In the experiments at 140 °C the material is mostly velocity strengthening, but exhibits unstable slip especially at high effective normal stress implying velocity-weakening behaviour (Fig. 2l; sidebar marks range of stick–slip occurrence). At low effective normal stress, 'stick–slip' occurs at the slowest sliding velocities of 1 μm s^{-1}, and covers an increasingly broader velocity range as effective normal stress is increased (Supplementary Figs 3 and 5).

Microstructural observations

Backscattered electron imaging of deformed calcareous ooze samples that exhibited weakening and unstable slip shows remnants of a 60-μm-wide Riedel (R) shear, potentially a principal slip zone (PSZ in Fig. 3) characterized by extreme grain size reduction. Micrometre-scale subangular to subrounded clasts enclosed in a micro- to nanogranular matrix (Fig. 3b) point to cataclastic flow as the major deformation mechanism. Discrete microfaults occur near the boundary, where grains down to nanoscale occur within a narrow, 1–2-μm-thick slip zone (black arrow in Fig. 3b). Most probably a large portion of unstable (seismogenic) slip is accommodated here, as there are no prominent boundary shears, and other microfaults are rare. The bulk of the deformed sample is homogeneous gouge indicative of a rather ductile, delocalized deformation. Unfortunately the sample disintegrated into scales when recovered, making more extensive study difficult. Sample recovery should be improved in a future study, so that better insight can be gained into representative shear band structure and internal deformation mechanisms using more sophisticated analytical methods.

Mechanisms for weakening and unstable slip

Recent research showed that highly reflective slip surfaces resembling natural polished fault planes in limestones form within simulated calcite gouge deformed in friction experiments conducted at similar velocities to those used here[27]. Polished slip surfaces were reported to consist of ductilely aligned nanogranular chains or fibres. It was inferred that a fault-slip mechanism resembling classical Ashby–Verrall superplasticity potentially produced unstable fault slip. We observed the same mirror-like slip surfaces within the deformed calcareous ooze gouge, suggesting similar slip mechanisms. Velocity-weakening behaviour by such mechanisms can result from the interaction between dilatation caused by grain-neighbour swapping and compaction by diffusive mass transfer within the principal slip zone according to the Niemeijer–Spiers mechanism for granular flow at the submicrometre scale[28]. The required anomalously high diffusion rates are common within nanosized materials and were related to temperatures above 80–100 °C where velocity weakening occurred[27]. Such a mechanism may therefore also have operated in our experiments.

However, the exact process responsible for the temperature and fluid-induced decrease in the internal friction coefficient of the present carbonate samples remains elusive. Increasing pore-fluid pressure potentially affects the gelification of silica or the solubility of calcite. Silica gel is an ultralow-friction material and regarded as a fault lubricant, since it was experimentally shown that formation of silica gel tribolayers results in a dramatic decrease of the friction coefficient[29–31]. The processes of silica gel formation and lubrication are still poorly understood, but it is possible that strained Si–O–Si bridges in amorphous silica preferentially react with water to form silica gel[29]. The opal in our samples is a potential source for rapid silica gel formation. As opal is also present in similar amounts in the hemipelagic clay, though, it cannot be the critical factor that accounts for the weakening of the carbonate gouge. Alternatively, the high fluid pressure somehow causes more effective intergranular lubrication by the fluid phase or a decrease in grain boundary frictional interaction, for example due to enhanced solubility and diffusion or enhanced defect motion at grain boundary nano-aspertites. As increased weakening occurred only at elevated temperature, initiation of microplasticity may also play a key role as indicated by the development of a pronounced crystallographic preferred orientation within principal slip zones[32]. To better understand the physico-chemical processes that control the observed weakening, further testing using differing pore-fluid compositions, for example, systematically varying the CO_2 content, and other parameters, is required. The rates of dissolution and reprecipitation of calcite depend on temperature, pH and CO_2 concentration within the fluid, and these therefore potentially affect solution transfer processes. CO_2 (partial) pressure has been experimentally shown to accelerate creep of wet calcite, especially towards smaller grain sizes[33].

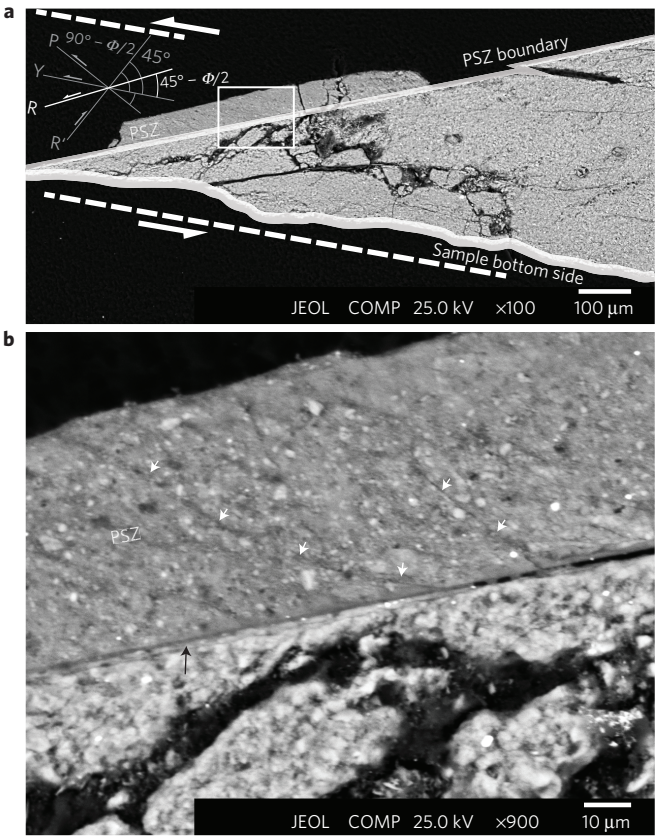

Figure 3 | Backscattered electron images of experimentally deformed calcareous ooze gouge. a, Remnants of a 60-μm-thick micro- to nanogranular Riedel (R) shear zone indicative of a principal slip zone (PSZ) within the gouge (see inset in upper left corner for orientations and related slip directions of R, R′, P, and Y-shears[45]); detail (white rectangle) is shown in **b**. Dashed lines with shear sense arrows indicate shear zone contact with the top and bottom pistons. **b**, The proposed PSZ consists of subangular micrometre-sized clasts within a nanogranular matrix. Discrete microfaults (white arrows) originate in the PSZ boundary region, which is a 1–2 μm thin slip plane (black arrow) with very small (non-resolvable) grains.

Décollement localization and earthquake nucleation

Localization of the plate-boundary fault zone, or décollement, within structurally weak and frictionally unstable material at

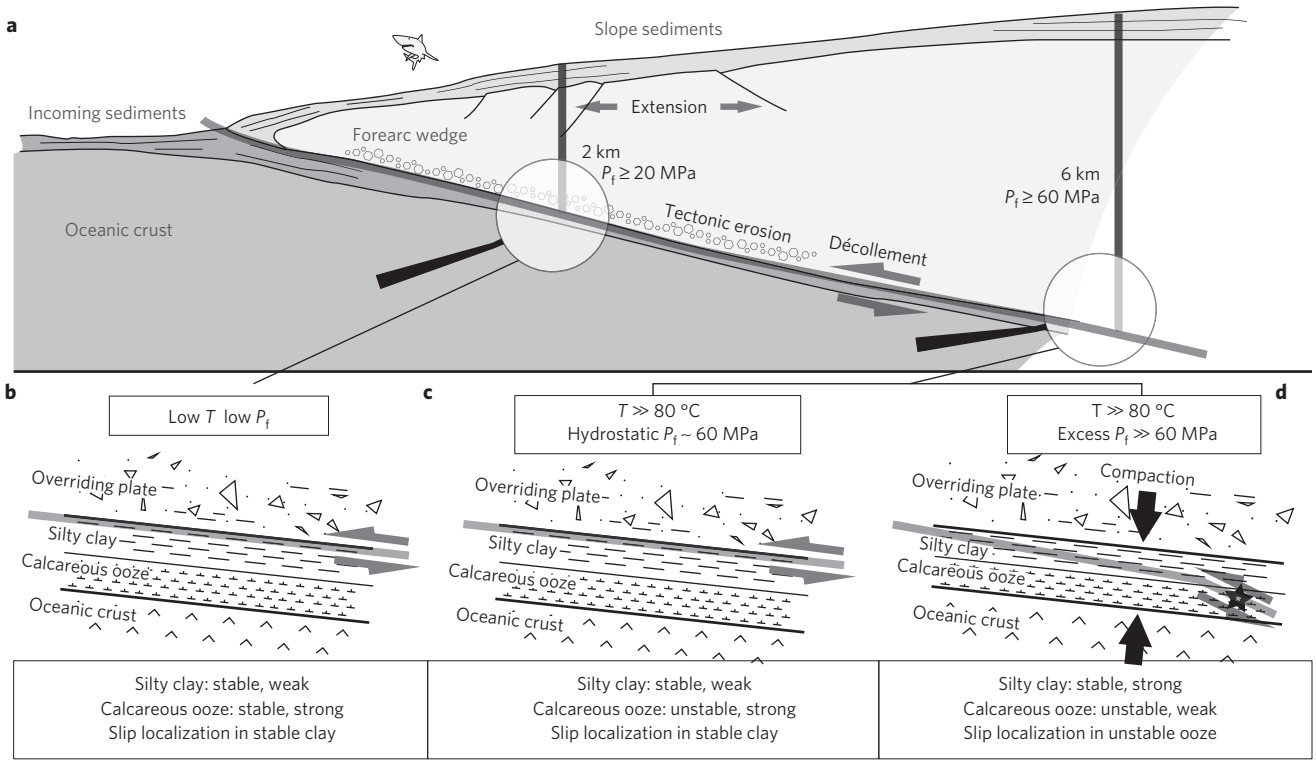

Figure 4 | Schematic sections across the forearc wedge of the Central American Subduction Zone offshore Costa Rica. a, Schematic section through the plate-boundary décollement zone; pore-pressure values are minimum estimates assuming hydrostatic conditions. **b**–**d**, Close-ups for the initial deformation condition in the upper part of the subduction channel (**b**) and two possibly intermittent conditions of hydrostatic/low pore-fluid pressure (**c**) and high/excess pore-fluid pressure (**d**) further downward at the upper end of the seismogenic zone. Consequences for localization and mode of slip are discussed in the text.

seismogenic depths, is a crucial prerequisite for fault reactivation and earthquake nucleation, respectively[34,35]. Ikari *et al.*[13] were the first to observe frictionally unstable behaviour in highly calcareous sediments and suggested their key role in governing earthquake nucleation during subduction. The sedimentary cover sequence entering the trench on top of a downgoing plate is usually well stratified and, especially in shallow ocean basins at low latitudes, contains pelagic calcareous ooze covered by hemipelagic sediments. These sediments are incorporated into the subduction channel in both accretionary and erosive continental margins, as indicated schematically in Fig. 4. At erosive margins such as the MAT, carbonate platforms on the continental shelf represent an alternative source of calcareous sediments, to be incorporated into the subduction channel by tectonic erosion. Indeed, through transient tectonic erosion and accretion, the forearc wedge of the Costa Rica erosive margin contains a pre- and early Miocene palaeo-accretionary prism that incorporates previously accreted calcareous sediments[36]. These may also end up in the subduction channel and subsequently control deformation and seismogenesis there.

The subduction décollement and associated faults are expected to localize in the weakest material present. This concept has been used to predict at which depth a frontal thrust cuts into the incoming sedimentary sequence, thereby determining the character of the subduction zone as erosive or accretionary[37]. Calcite gouge is known to exhibit much higher shear strength than clayey gouges[13,38–40], so is less prone to hosting localization of slip. It was suggested that exposed chalk on local topographic highs, for example seamounts, might act as asperities in which earthquakes may nucleate[13]. Our new results on similar material unveil a systematic weakening of calcareous ooze gouge in response to increasing pore-fluid pressures and temperatures (Fig. 2d–f). Since the internal friction of clay-rich samples remains constant over the entire range of tested conditions, the shear strength of samples derived from calcareous ooze eventually falls to much lower values, allowing for slip localization in the calcareous sediments (Fig. 4b–d). At the MAT, deformation partitioning into the calcareous sediments of the forearc wedge would also be feasible in association with an upward movement of the plate-boundary fault and tectonic erosion of the wedge.

A large portion of the fluids entering subduction zones is located in the pore space of incoming sediments[41,42]. Expulsion of these fluids occurs via compaction, usually during the first ~3–7 km of rapid burial[42]. This process reduces porosity, increases sediment stiffness and can generate significant excess pore-fluid pressure (Fig. 4b–d). Frictional instability in our experiments is observed between 70 °C, where predominantly stable sliding occurs (Fig. 2k), and 140 °C, where stick–slips occur, in line with the previous findings of Verberne *et al.*[32], whose results on both dry and wet calcite gouge show a transition from stable to (potentially) unstable sliding above 80–100 °C. Such temperatures characterize the updip limit of seismogenesis[41,43,44].

In summary, we propose that thermally induced frictional instability together with the combined effects of temperature- and pore-fluid-pressure-dependent weakening of carbonate-rich fault gouges (>85% calcite) means that carbonates are potentially important host rocks for the nucleation of subduction thrust earthquakes at low latitudes, especially in shallow seismogenesis. Once initiated, rupture nucleation is probably accompanied and/or followed by near-instantaneous dilatation and dissipation of excess pore-fluid pressure, resulting in immediate re-strengthening and seismogenic rupture propagation into adjacent clay-rich sediments that can accommodate large slip. Only there, slip will ultimately reach coseismic velocities with associated frictional heating and thermal pressurization.

Methods

Methods, including statements of data availability and any associated accession codes and references, are available in the online version of this paper.

Received 7 December 2015; accepted 30 June 2016; published online 1 August 2016

References

1. Archer, D. E. An atlas of the distribution of calcium carbonate in sediments of the deep sea. *Glob. Biogeochem. Cycles* **10,** 159–174 (1996).
2. Byrne, D. E., Davis, D. M. & Sykes, L. R. Loci and maximum size of thrust earthquakes and the mechanics of the shallow region of subduction zones. *Tectonics* **7,** 833–857 (1988).
3. Toshiko, S., Seno, T. & Uyeda, S. A simple rheological framework for comparative subductology. *Relating Geophys. Struct. Process.* **76,** 39–52 (1993).
4. Hyndman, R. D. & Wang, K. Thermal constraints on the zone of major thrust earthquake failure—the cascadia subduction zone. *J. Geophys. Res.* **98,** 2039–2060 (1993).
5. Moreno, M. *et al*. Locking of the Chile subduction zone controlled by fluid pressure before the 2010 earthquake. *Nature Geosci.* **7,** 292–296 (2014).
6. Audet, P., Bostock, M. G., Christensen, N. I. & Peacock, S. M. Seismic evidence for overpressured subducted oceanic crust and megathrust fault sealing. *Nature* **457,** 76–78 (2009).
7. Ito, Y., Obara, K., Matsuzawa, T. & Maeda, T. Very low frequency earthquakes related to small asperities on the plate boundary interface at the locked to aseismic transition. *J. Geophys. Res.* **114,** B00A13 (2009).
8. Brown, K. M., Tryon, M. D., DeShon, H. R., Dorman, L. M. & Schwartz, S. Y. Correlated transient fluid pulsing and seismic tremor in the Costa Rica subduction zone. *Earth Planet. Sci. Lett.* **238,** 189–203 (2004).
9. DenHartog, S. A. M., Niemeijer, A. R. & Spiers, C. J. New constraints on megathrust slip stability under subduction zone P-T conditions. *Earth Planet. Sci. Lett.* **353,** 240–252 (2012).
10. DenHartog, S. A. M., Peach, C. J., de Winter, D. A. M., Spiers, C. J. & Shimamoto, T. Frictional properties of megathrust fault gouges at low sliding velocities: new data on effects of normal stress and temperature. *J. Struct. Geol.* **38,** 156–171 (2012).
11. Namiki, Y., Tsutsumi, A., Ujiie, K. & Kameda, J. Frictional properties of sediments entering the Costa Rica subduction zone offshore the Osa Peninsula: implications for fault slip in shallow subduction zones. *Earth Planet. Space* **66,** 72 (2014).
12. Saffer, D. M. & Marone, C. Comparison of smectite- and illite-rich gouge frictional properties: application to the updip limit of the seismogenic zone along subduction megathrusts. *Earth Planet. Sci. Lett.* **215,** 219–235 (2003).
13. Ikari, M. J., Niemeijer, A. R., Spiers, C. J., Kopf, A. J. & Saffer, D. M. Experimental evidence linking slip instability with seafloor lithology and topography at the Costa Rica convergent margin. *Geology* **41,** 891–894 (2013).
14. Ikari, M. J., Saffer, D. M. & Marone, C. Effect of hydration state on the frictional properties of montmorillonite-based fault gouge. *J. Geophys. Res.* **112,** B06423 (2007).
15. Morrow, C. A., Shi, C. & Byerlee, J. D. Strain-hardening and strength of clay-rich fault gouges. *J. Geophys. Res.* **87,** 6771–6780 (1982).
16. Ranero, C. R. & von Huene, R. Subduction erosion along the Middle America convergent margin. *Nature* **404,** 748–752 (2000).
17. Clift, P. & Vannucchi, P. Controls on tectonic accretion versus erosion in subduction zones: implications for the origin and recycling of the continental crust. *Rev. Geophys.* **42,** RG2001 (2004).
18. Ranero, C. R. *et al*. A cross section of the convergent Pacific margin of Nicaragua. *Tectonics* **19,** 335–357 (2000).
19. Langseth, M. G., Cann, J. R., Natland, J. H. & Hobart, M. Geothermal phenomena at the Costa-Rica Rift—background and objectives for drilling at deep-sea drilling Project Site-501, Site-504, and Site-505. *Initial Rep. Deep Sea Drill. Project* **69,** 5–29 (1983).
20. von Huene, R. *et al*. A summary of Deep Sea Drilling Project Leg 67 shipboard results from the Mid-America Trench transect off Guatemala. *Geol. Soc.* **10,** 121–129 (1982).
21. Expedition 344 Scientists Costa Rica Seismogenesis Project, Program A Stage 2 (CRISP-A2): sampling and quantifying lithologic inputs and fluid inputs and outputs of the seismogenic zone. *IODP Prel. Rept.* **344,** 1–81 (2013).
22. Niemeijer, A. R., Spiers, C. J. & Peach, C. J. Frictional behaviour of simulated quartz fault gouges under hydrothermal conditions: results from ultra-high strain rotary shear experiments. *Tectonophysics* **460,** 288–303 (2008).
23. Dieterich, J. H. Modeling of rock friction: 1. Experimental results and constitutive equations. *J. Geophys. Res.* **84,** 2161 (1979).
24. Ruina, A. Slip instability and state variable friction laws. *J. Geophys. Res.* **88,** 10359–10370 (1983).
25. Gu, J.-C., Rice, J. R., Ruina, A. L. & Tse, S. T. Slip motion and stability of a single degree of freedom elastic system with rate and state dependent friction. *J. Mech. Phys. Solids* **32,** 167–196 (1984).
26. Brace, W. F. & Byerlee, J. D. Stick-slip as a mechanism for earthquakes. *Science* **153,** 990–992 (1966).
27. Verberne, B. A., Plümper, O., de Winter, D. A. M. & Spiers, C. J. Superplastic nanofibrous slip zones control seismogenic fault friction. *Science* **346,** 1342–1344 (2014).
28. Niemeijer, A. R. & Spiers, C. J. A microphysical model for strong velocity weakening in phyllosilicate-bearing fault gouges. *J. Geophys. Res.* **112,** B10405 (2007).
29. Goldsby, D. L. & Tullis, T. E. Low frictional strength of quartz rocks at subseismic slip rates. *Geophys. Res. Lett.* **29,** 1844 (2002).
30. Nakamura, Y. *et al*. Amorphization of quartz by friction: implication to silica-gel lubrication of fault surfaces. *Geophys. Res. Lett.* **39,** L21303 (2012).
31. Di Toro, G., Goldsby, D. L. & Tullis, T. E. Friction falls towards zero in quartz rock as slip velocity approaches seismic rates. *Nature* **427,** 436–439 (2004).
32. Verberne, B. A. *et al*. Nanocrystalline slip zones in calcite fault gouge show intense crystallographic preferred orientation: crystal plasticity at sub-seismic slip rates at 18–150 °C. *Geology* **41,** 863–866 (2013).
33. Liteanu, E., Niemeijer, A., Spiers, C. J., Peach, C. J. & de Bresser, J. H. P. The effect of CO_2 on creep of wet calcite aggregates. *J. Geophys. Res.* **117,** B03211 (2012).
34. Faulkner, D. R., Mitchell, T. M., Behnsen, J., Hirose, T. & Shimamoto, T. Stuck in the mud? Earthquake nucleation and propagation through accretionary forearcs. *Geophys. Res. Lett.* **38,** L18303 (2011).
35. Stipp, M. *et al*. Strong sediments at the deformation front, and weak sediments at the rear of the Nankai accretionary prism, revealed by triaxial deformation experiments. *Geochem. Geophys. Geosyst.* **14,** 4791–4810 (2013).
36. Vannucchi, P., Fisher, D. M., Bier, S. & Gardner, T. W. From seamount accretion to tectonic erosion: formation of Osa Mélange and the effects of Cocos Ridge subduction in southern Costa Rica. *Tectonics* **25,** TC2004 (2006).
37. Kopf, A. Effective strength of incoming sediments and its implications for plate boundary propagation: Nankai and Costa Rica as type examples of accreting vs. erosive convergent margins. *Tectonophysics* **608,** 958–969 (2013).
38. Shimamoto, T. & Logan, J. M. Effects of simulated clay gouges on the sliding behavior of Tennessee sandston. *Tectonophysics* **75,** 243–255 (1981).
39. Verberne, B. A., He, C. & Spiers, C. J. Frictional properties of sedimentary rocks and natural fault gouge from the Longmen Shan fault zone, Sichuan, China. *Bull. Seismol. Soc. Am.* **100,** 2767–2790 (2010).
40. Verberne, B. A. *et al*. Frictional properties and microstructure of calcite-rich fault gouges sheared at sub-seismic sliding velocities. *Pure Appl. Geophys.* **171,** 2617–2640 (2014).
41. Saffer, D. M. & Tobin, H. J. Hydrogeology and mechanics of subduction zone forearcs: fluid flow and pore pressure. *Annu. Rev. Earth Planet. Sci.* **39,** 157–186 (2011).
42. Bekins, B. A. & Dreiss, S. J. A simplified analysis of parameters controlling dewatering in accretionary prisms. *Earth Planet. Sci. Lett.* **109,** 275–287 (1992).
43. Hyndman, R. D., Yamano, M. & Oleskevich, D. A. The seismogenic zone of subduction thrust faults. *Island Arc* **6,** 244–260 (1997).
44. Völker, D., Grevemeyer, I., Stipp, M., Wang, K. & He, J. Thermal control of the seismogenic zone of southern central Chile. *J. Geophys. Res.* **116,** B10305 (2011).
45. Riedel, W. Zur Mechanik geologischer Brucherscheinungen. *Zentralbl. Mineral. Geol. Palaeontol* **1929B,** 354–368 (1929).

Acknowledgements

This research used data and samples provided by the Integrated Ocean Drilling Program (IODP). M.S. thanks the Shipboard Parties of IODP Expeditions 334 and 344 for their great colleagueship and their commitment aboard DV *JOIDES Resolution*. R.M.K. greatly appreciated experimental help by M. Sawai, quantitative analysis of diffractograms by R. Kuehn and insight into unpublished data from D. Charpentier. Financial support by Deutsche Forschungsgemeinschaft (DFG) through grant STI298/7-1,2 to M.S. and J.H.B. is kindly acknowledged. A.R.N. is supported by the Netherlands Organisation for Scientific Research (NWO) through a VIDI grant (no. 854.12.011) and by the ERC starting grant SEISMIC (no. 335915).

Author contributions

R.M.K. conducted experiments and data analysis in collaboration with A.R.N. M.S. initiated the project. All authors contributed to discussion and writing the manuscript.

Additional information

Supplementary information is available in the online version of the paper. Reprints and permissions information is available online at www.nature.com/reprints. Correspondence and requests for materials should be addressed to R.M.K.

Competing financial interests

The authors declare no competing financial interests.

Methods

Representative starting material compositions were derived from the powder diffraction data of the IODP LIMS Reports online repository (http://web.iodp.tamu.edu/UWQ). The calcite contents were calculated from related ion chromatography data assuming that all carbonate is calcium carbonate. These compositional data measured by the IODP expedition 344 shipboard party onboard DV *JOIDES Resolution* are in good agreement with our observations from backscattered electron imaging and energy dispersive X-ray spectroscopy using a JEOL JXA 8200 electron microprobe on our starting material (see Supplementary Methods for diffractograms and backscattered electron images).

Rotary shear experimental samples were dried at 55 °C for 24 h to avoid dehydration reactions, disaggregated by mortar and pestle and sieved to a grain size <125 μm. During each experiment, the effective normal stress was increased between 30 MPa and 110 MPa in steps of 20 MPa. Before shearing, the system was left to equilibrate at the desired temperature and pore-fluid pressure conditions for at least 45 min in heated experiments. At each effective stress state, a series of slip velocity steps was performed following the scheme 10-1-3-10-30-100 μm s^{-1}. The first velocity step at 10 μm s^{-1} served to establish a starting microstructure and steady-state friction coefficient at experimental conditions. To obtain the individual rate-and-state friction parameters, we employed a least-squares minimization, inverse modelling technique to fit Dieterich's slowness law to our experimental data, correcting for superimposed slip hardening/weakening trends[46] (Fig. 1b). The fitted relation took the form:

$$(\tau/\sigma_n^{eff}) = (\tau/\sigma_n^{eff})_0 + a\ln(V/V_0) + b_1\ln(V_0\Theta_1/Dc_1) + b_2\ln(V_0\Theta_2/Dc_2) \quad (4)$$

where $(\tau/\sigma_n^{eff})_0$ and V_0 are the reference steady-state friction coefficient and the sliding velocity before a velocity step, a, b_1 and b_2 are material properties, and the Θ_i are state variables that evolve according to:

$$d\Theta_i/dt = 1 - V\Theta_i/D_{ci}, i = 1,2 \quad (5)$$

Employing two state variables Θ_1 and Θ_2 results in a better fit of the friction evolution model following a velocity perturbation. In cases in which this numerical approach failed due to experimental artefacts or noisy records, (a–b) was obtained using equation (1), which is the simplified equation for steady state. In Fig. 2g–l, such data points are indicated by dashed symbols. Since inverting for data of velocity steps that show stick–slip is problematic, the effective normal stress range of stick–slip occurrence is marked by a sidebar in Fig. 2l. Initial gouge thickness of ~2 mm and a total displacement of up to 42 mm translate into a minimum accumulated shear strain of $\gamma \sim 20$ after each experiment. Due to gouge compaction under load and continuous thinning during shear, the true strain value was in fact much higher.

Data availability. The data that support the findings of this study are available from the corresponding author on request.

References

46. Reinen, L. A. & Weeks, J. D. Determination of rock friction constitutive parameters using an iterative least squares inversion method. *J. Geophys. Res.* **98,** 15937–15950 (1993).